The Astrophysical Journal Letters, 908:L31 (7pp), 2021 February 20 https://doi.org/10.3847/2041-8213/abdebd

Fiery Cores: Bursty and Smooth Star Formation Distributions across Galaxy Centers in Cosmological Zoom-in Simulations

Matthew E. Orr[1,2,3], H Perry Hatchfield[4], Cara Battersby[4], Christopher C. Hayward[3], Philip F. Hopkins[1], Andrew Wetzel[5], Samantha M. Benincasa[8,9], Sarah R. Loebman[5,10], Mattia C. Sormani[6], and Ralf S. Klessen[6,7]
[1] TAPIR, Mailcode 350-17, California Institute of Technology, Pasadena, CA 91125, USA; matt.orr@rutgers.edu
[2] Department of Physics and Astronomy, Rutgers University, 136 Frelinghuysen Road, Piscataway, NJ 08854, USA
[3] Center for Computational Astrophysics, Flatiron Institute, 162 Fifth Avenue, New York, NY 10010, USA
[4] University of Connecticut, Department of Physics, 196A Auditorium Road, Unit 3046, Storrs, CT 06269, USA
[5] Department of Physics, University of California, Merced, CA 95343, USA
[6] Universität Heidelberg, Interdisziplinäres Zentrum für Astronomie, Institutfür Theoretische Astrophysik, Albert-Ueberle-Str. 2, D-69120 Heidelberg, 11, Germany
[7] Universität Heidelberg, Interdisziplinäres Zentrum für Wissenschaftliches Rechnen, Im Neuenheimer Feld 205, D-69120 Heidelberg, 13, Germany
[8] Center for Cosmology and AstroParticle Physics (CCAPP), The Ohio State University, Columbus, OH 43210, USA
[9] Department of Astronomy, The Ohio State University, Columbus, OH 43210, USA
Received 2020 December 4; revised 2021 January 20; accepted 2021 January 21; published 2021 February 19

Abstract

We present an analysis of the $R \lesssim 1.5$ kpc core regions of seven simulated Milky Way-mass galaxies, from the FIRE-2 (Feedback in Realistic Environments) cosmological zoom-in simulation suite, for a finely sampled period ($\Delta t = 2.2$ Myr) of 22 Myr at $z \approx 0$, and compare them with star formation rate (SFR) and gas surface density observations of the Milky Way's Central Molecular Zone (CMZ). Despite not being tuned to reproduce the detailed structure of the CMZ, we find that four of these galaxies are consistent with CMZ observations at some point during this 22 Myr period. The galaxies presented here are not homogeneous in their central structures, roughly dividing into two morphological classes; (a) several of the galaxies have very asymmetric gas and SFR distributions, with intense (compact) starbursts occurring over a period of roughly 10 Myr, and structures on highly eccentric orbits through the CMZ, whereas (b) others have smoother gas and SFR distributions, with only slowly varying SFRs over the period analyzed. In class (a) centers, the orbital motion of gas and star-forming complexes across small apertures ($R \lesssim 150$ pc, analogously $|l| < 1^\circ$ in the CMZ observations) contributes as much to tracers of star formation/dense gas appearing in those apertures, as the internal evolution of those structures does. These asymmetric/bursty galactic centers can simultaneously match CMZ gas and SFR observations, demonstrating that time-varying star formation can explain the CMZ's low star formation efficiency.

Unified Astronomy Thesaurus concepts: Galactic center (565); Star formation (1569); Interstellar medium (847); Spiral galaxies (1560); Galaxy kinematics (602); Stellar feedback (1602)

1. Introduction

Within the context of empirical star formation laws, galaxy centers often exhibit particularly extreme and peculiar properties. From observations on scales averaging over entire galaxies down to those of ∼100 pc, the star formation rate (SFR) scales with the surface density of molecular gas as a power-law relationship known as the Kennicutt–Schmidt law (KS; Schmidt 1959; Kennicutt 1998). Moreover, the presence of high density ($>10^4$ cm^{-3}) gas seems to strongly predict the star formation rate on the scale of individual molecular clouds (Lada et al. 2010, 2012). Some galaxy centers host nuclear starbursts (e.g., NGC 253; Leroy et al. 2018), whereas the Milky Way's central region, known as the Central Molecular Zone (CMZ) appears to be underproducing stars relative to its dense gas content, with surveys finding an SFR 10–100 times lower than that predicted by contemporary theory (e.g., Immer et al. 2012; Longmore et al. 2013). This deficiency has motivated many studies of the star-forming properties of molecular clouds in this extreme environment (Rathborne et al. 2014; Ginsburg et al. 2018; Walker et al. 2018; Barnes et al. 2019; Henshaw et al. 2019).

While there is resilient evidence for this star formation deficiency in the Milky Way's CMZ (Barnes et al. 2017), there are still signs of ongoing and previously more intense past star formation episodes within the past 2–6 Myr (e.g., Liermann et al. 2012; Lu et al. 2013; Clark et al. 2019). It has been suggested that the CMZ may have previously been in a more vigorous state of star formation, perhaps similar to other galaxies with nuclear starbursts (Kruijssen et al. 2014; Krumholz et al. 2017; Sormani & Li 2020). Arguments that the CMZ has a low star formation efficiency per dense gas mass often presuppose that the CMZ is in equilibrium, and the time evolution of galactic centers is difficult to study using Milky Way observations alone.

Although limited to probing scales from 10 to 100 pc, extragalactic galaxy center studies have measured star formation and gas in MW-mass galaxy centers across a range of conditions (Casasola et al. 2015; Gallagher et al. 2018, among others). These observations have highlighted the variety of conditions under which star formation occurs in galaxy centers, further suggesting that large variations (∼dex) in SFRs and gas surface densities naturally arise (Leroy et al. 2013) in these extreme environments.

Exploring the nature of star formation in galactic centers requires detailed modeling of star formation and feedback processes (e.g., Armillotta et al. 2019), as well as a self-consistent picture of gas dynamics in the full context of galactic structure and evolution (e.g., Sormani et al. 2020; Tress et al. 2020). Cosmological zoom-in simulations have begun to meet

[10] Hubble Fellow.

these physics requirements, and now have adequate spatial/mass resolution to follow the multiphase turbulent ISM, and capture the cosmological context of Milky Way–like galaxies (e.g., Hopkins et al. 2014, 2018). In particular, work within the FIRE collaboration has been able to explore star formation in the context of galactic disks, cloud lifetimes, and SMBH–gas dynamics connections (Anglés-Alcázar et al. 2017; Orr et al. 2018, 2020; Benincasa et al. 2020; Gurvich et al. 2020). Recent work by Sanderson et al. (2020) has compared several galaxies in the FIRE-2 suite in detail to properties of the MW.

In this Letter, we compare the centers of seven FIRE-2 galaxies (Wetzel et al. 2016; Hopkins et al. 2018), all approximately Milky Way–mass spirals, with Milky Way CMZ and extragalactic observations. These simulations have $z = 0$ SFRs of 3–10 $M_\odot\,\mathrm{yr}^{-1}$, which is more typical of $L^\star$ galaxies compared to the MW (our Galaxy appears to be an outlier to lower SFR; Longmore et al. 2013). Specifically, we map the centers of the simulated galaxies at high spatial resolution to understand the effects of dynamical evolution and feedback over a short (∼22 Myr) timescale on proxies for SFR and gas surface density tracers, and subsequent interpretations of star formation activity in their central regions.

2. Methods

We analyze the central regions of the seven Milky Way/Andromeda-mass spiral galaxies from the "standard physics" Latte suite of FIRE-2 simulations introduced in Wetzel et al. (2016) and Hopkins et al. (2018). The spatially resolved properties of the gas surface densities, velocity dispersions, and SFRs across the disks of these galaxies have been studied in detail in Orr et al. (2020). This work makes use of 11 snapshots finely spaced in time ($\Delta t \approx 2.2$ Myr) at $z \approx 0$ for each of the simulations. A brief summary of the $z \approx 0$ global properties of the galaxy simulations are included in Table 1 of Orr et al. (2020).

The simulations analyzed here all have minimum baryonic particle masses of $m_{b,\mathrm{min}} = 7100\ M_\odot$, minimum adaptive force softening lengths <1 pc, and a 10 K gas temperature floor. With adaptive softening lengths, we note that the median softening length within the disk in the runs at $z = 0$ is $h \sim 20$–40 pc (at a $n \sim 1\ \mathrm{cm}^{-3}$), with the dense turbulent disk structures having necessarily shorter softening lengths. The aperture sizes considered in this work are 145–500 pc,[11] and so are well above the minimum resolvable scales in the simulations.

Importantly, for discussion here, star formation in the simulations occurs on a freefall time in gas which is dense ($n > 10^3\ \mathrm{cm}^{-3}$), molecular (per the Krumholz & Gnedin 2011 prescription), self-gravitating (viral parameter $\alpha_{\mathrm{vir}} < 1$), and Jeans-unstable below the resolution scale. Once these requirements are met, the SFR at the particle scale is assumed to be $\dot{\rho}_\star = \rho_{\mathrm{H_2}}/t_{\mathrm{ff}}$ (i.e., 100% efficiency per freefall time). Star particles are treated as single stellar populations, with known age, metallicity, and mass. Feedback from supernovae, stellar mass loss (OB/AGB-star winds), photoionization and photoelectric heating, and radiation pressure are explicitly modeled. These simulations do not include any supermassive black holes (SMBHs), and accordingly do not have any feedback associated with BH accretion, nor do they include cosmic rays or other MHD physics. Detailed descriptions of these physics and their implementation can be found in Hopkins et al. (2018).

We produce mock observational maps from the snapshots using the same methods as Orr et al. (2018, 2020): we project the galaxies face-on according to their stellar angular momentum vector (including star particles out to 20 kpc) and bin star particles and gas elements into square pixels with side lengths (i.e., "pixel sizes") 25 pc. The maps analyzed here are 3 kpc on a side, and integrate gas and stars within ±1.5 kpc of the galactic midplane.

We generate a proxy for observational measures of recent SFRs by calculating the 10 Myr-averaged SFR in the pixels. We do this by summing the mass of star particles with ages less than 10 Myr, and correcting for mass loss from stellar winds and evolutionary effects using predictions from STARBURST99 (Leitherer et al. 1999). This time interval was chosen for its approximate correspondence with the timescales traced by recombination lines like Hα (Kennicutt & Evans 2012).[12] To compare with gas observations, we calculate column densities for the "cold and dense" gas ($\Sigma_{\mathrm{C\&D}}$ throughout) with $T < 500$ K and $n_{\mathrm{H}} > 1\ \mathrm{cm}^{-3}$. This gas reservoir taken as a proxy for the cold molecular gas in the simulations following the methodology of Orr et al. (2020), and ought roughly to correspond with gas traced by cold dust or CO observations in the CMZ.

3. Results

In this sample of only seven FIRE-2 Milky Way analogs, there is a surprising variety of conditions in their centers. As an example of properties seen in the galaxy centers, Figure 1 shows 8.8 Myr of two of the FIRE-2 galaxies (m12b and m12m), and how their SFRs and gas surface densities evolve within their central ∼500 pc (zoomed insets). Despite having similar masses of cold gas in their galactic centers, the two simulations have morphologically distinct central regions, in terms of their cold gas distributions and star-forming complexes. Of the two galaxies in Figure 1, only m12b is able to match observational estimates using YSO counts and HII regions of the CMZ SFR within $|l| < 1°$ (Longmore et al. 2013), specifically this is seen to occur during an inter-starburst period (at $t = 8.9$ Myr, center-left column). At least four of the FIRE galaxies (m12b, m12f, m12m, and m12r) match CMZ SFR and gas surface density properties concurrently at some time in this 22 Myr period.

3.1. Two Morphological Classes of FIRE-CMZs

The FIRE galaxies presented here cover a range of morphologies in their centers because these simulations were not designed to match the detailed structural properties of our Galactic center. Within the sample of seven galaxies, we see two distinct classes of central morphology in their fiery cores (gas and star formation distributions within $R \approx 1.5$ kpc):

[11] For comparison with CMZ observations, a physical radial extent of $R \lesssim 145$ pc corresponds to $|l| \lesssim 1°$ in Galactic longitude, assuming a distance of $d \approx 8.2$ kpc.

[12] A direct comparison to observations, by post-processing the snapshots to explicitly model Hα, would make for a more accurate modeling, but accounting for, e.g., dust and other complexities, is beyond this Letter's scope, where we wish to focus on the "true" SFRs and their spatial distributions. Work by Velázquez et al. (2021) has suggested that shorter (∼5 Myr) timescales more accurately trace Hα emission. We use a slightly longer averaging window such that the simulations well-resolve SFR estimates of the CMZ over these timescales within $R < 145$ pc (where ∼10 young star particles corresponds to a measured SFR of ∼0.1 $M_\odot\ \mathrm{yr}^{-1}\ \mathrm{kpc}^{-2}$), and are more conservative in our sensitivity to SFR variability.

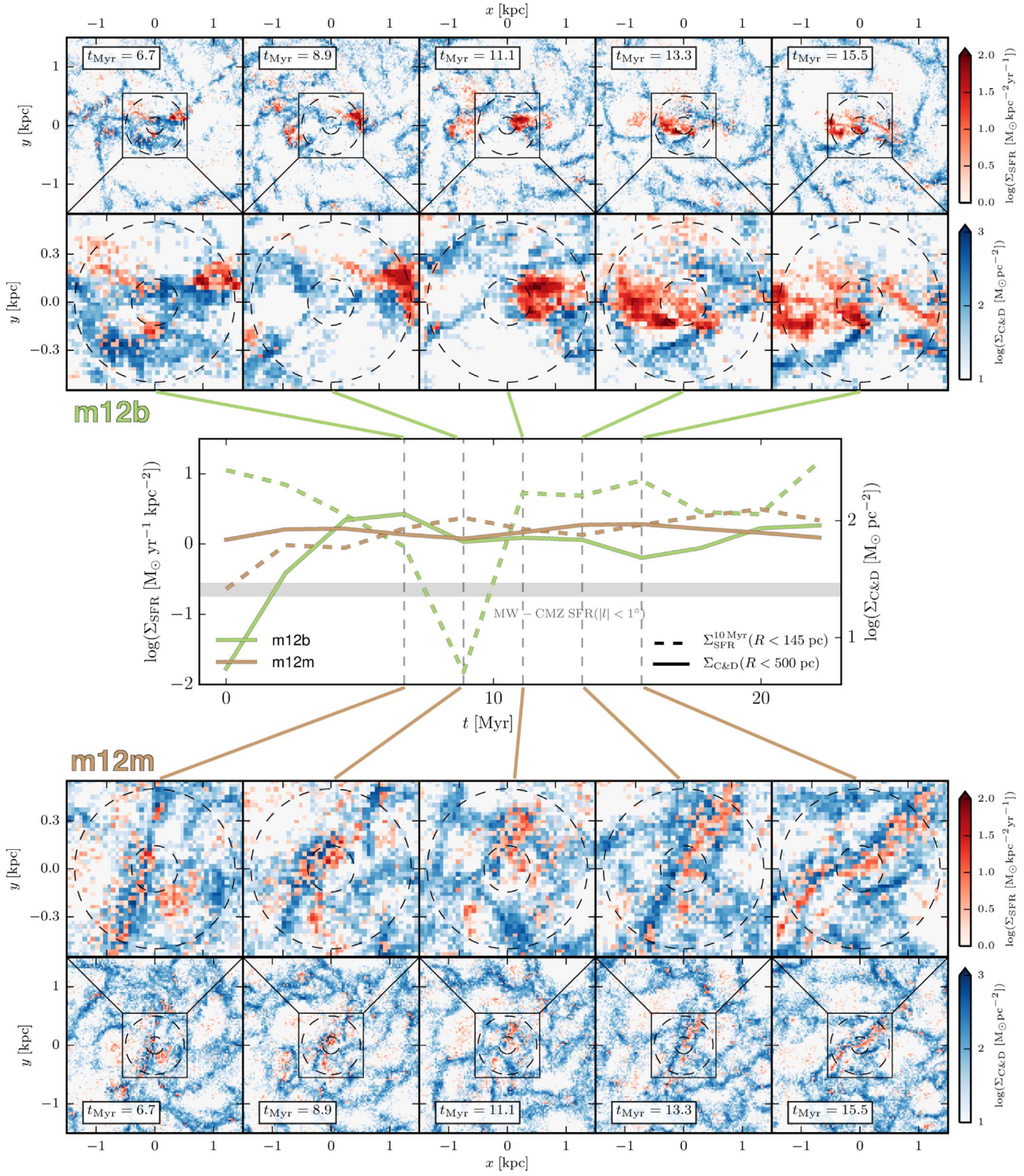

Figure 1. Face-on central regions of two FIRE-2 spiral galaxies at five snapshots in time (advancing right, $\Delta t \approx 2.2$ Myr): m12b (top subfigure) and m12m (bottom subfigure), cold and dense gas (C&D, $T < 500$ K and $n_{\rm H} > 1$ cm^{-3}) in blues with 10 Myr-averaged SFR (reds) overlaid, with 25 pc pixel sizes. Outermost rows show 3 kpc regions, with inner rows showing 1.1 kpc zoom-ins. Zoomed-in panels show two apertures, with $R = 145$, 500 pc (inner, outer dashed lines, respectively). Middle panel shows the time evolution of SFRs within $R < 145$ pc (dashed lines) and gas surface densities within $R < 500$ pc (solid lines). MW CMZ SFR estimate with uncertainty ($|l| < 1°$ from Longmore et al. 2013) plotted as a horizontal gray-shaded band. Despite having similar gas surface densities on $R < 500$ pc scales (modulo m12b lacking C&D gas within ∼300 pc for the first ∼5 Myr), the two galaxies have markedly different star formation in their centers, with m12b (green lines) having bursty, intense star formation as opposed to the smoother cirrus of star formation seen in m12m (brown lines). The large SFR variation in m12b essentially corresponds to the evolution and physical motion of a single massive star-forming region.

(a) "Asymmetric/Bursty" (m12b, m12c, m12f, and m12w): Large, asymmetric gas clouds and star-forming complexes are seen. Star formation is concentrated in intense starbursts whose feedback dramatically shapes the local gas environment (see m12b, upper subfigure of Figure 1). Two simulations falling in this category (m12b and m12f) simultaneously match the MW CMZ gas and SFR measurements. The two others (m12c and m12w) do not simultaneously have SFR and dense gas tracers within the central 145 pc at any point in this time window.

(b) "Smooth" (m12i, m12m, and m12r): Gas and star formation is smoothly distributed within the galactic centers, with clear feeding of gas into center, and a cirrus of star formation (see m12m, lower subfigure of Figure 1). Feedback events do not dramatically alter the local gas environment, as the feedback is relatively dispersed across their centers.

Interestingly, none of the galaxies here exhibit the ring structures, presumed to be long-lived, seen by studies of the central regions of other spiral galaxies and the MW CMZ (Kormendy & Kennicutt 2004; Molinari et al. 2011). We note the lack of strong bars in the centers of any of these FIRE galaxies at this time (m12m did develop a strong bar around $z \approx 0.2$, but it does not survive to $z = 0$; Debattista et al. 2019); without the presence of bars in these simulations at $z = 0$, we cannot speak to the dynamical importance of bars in producing central galactic environments similar to the MW CMZ. Other work has highlighted the potential impacts of bars in funneling gas core-ward and forming rings (Sormani et al. 2015, 2018). However, bar-induced effects would likely push these simulated galactic centers toward more asymmetric states, supporting the idea that bursty, rather than steady-state, star formation is necessary to explain MW CMZ observations. Specifically, Sormani et al. (2018) showed that the gas flow in a barred potential naturally becomes turbulent and asymmetric, even in the absence of any type of stellar feedback. And so, we leave it to future work to investigate the gas flows driven in FIRE galaxies by the bars that form at higher redshift.

The structures in the centers of the FIRE galaxies appear to be fairly transient in nature, existing for $\lesssim$10 Myr (similar to the GMC lifetimes seen in these simulations more broadly by Benincasa et al. 2020). We should be clear: spiral structures do exist core-ward in these simulations (see the clear presence of spiral arms in both m12b and m12m in Figure 1). In the case of the class (a) morphologies, the central ($R < 300$ pc) gas structures are on visibly eccentric orbits through their CMZs (similar to MW CMZ orbital modeling by Kruijssen et al. 2015), and are disrupted by intense feedback following starbursts. Previous work with FIRE by Torrey et al. (2017) showed that star formation-feedback instabilities in galactic centers can arise when the local dynamical time becomes shorter than the feedback timescale. The class (b) morphologies have smoother gas distributions in their centers, and with the gentler, more dispersed feedback from diffuse star formation, are not as strongly disrupted. Owing perhaps to their smoother gas distributions, less of the gas is on very eccentric orbits ($\sim$5%–10% of gas having $v_{\rm in-plane} > \sqrt{2}\,v_c$, versus up to $\sim$20%–40% in the class (a) centers) and, to an extent, the structures are clearer continuations of spiral arms down to their centers. The difference between the two classes may, in the case of these FIRE galaxies, arise from more or less violent recent merger histories/interactions with (smaller) galaxies, with the class (b) galaxies having more quiescent recent histories. To wit, as shown in Garrison-Kimmel et al. (2018), m12i and m12m have not experienced any notable head-on major mergers.

One caveat to the discussion regarding these morphologies is the lack of SMBHs in these simulations. Work by Anglés-Alcázar et al. (2017) has investigated the influence of SMBHs on their immediate environments, and their ability to disrupt gas structures while they are actively accreting, may disallow the smooth central gas distributions within $\sim$100 pc in class (b). And so, class (a) galactic centers may be the more realistic central galactic environments.

3.2. Matching FIRE-CMZs with the Milky Way CMZ and External Galaxies

Figure 2 shows the evolution over 22 Myr of the SFR and cold and dense (C&D) gas surface densities, and derived depletion times, within $R = 500$ and 145 pc apertures (corresponding roughly to CMZ observations within $|l| \lesssim 3.^\circ5$ and 1°, with SFRs taken from Longmore et al. 2013 and gas from Mills & Battersby 2017) for the FIRE galaxies. Averaging over larger scales reduces the degree of scatter seen in SFR and gas surface density for each galaxy. However, as discussed in Section 3.1, the time evolutions of $\Sigma_{\rm SFR}$ and $\Sigma_{\rm C\&D}$ alone do not fully capture the idiosyncrasies of each galaxy. For example, m12r is relatively less massive ($\sim$4×) and has a smaller cold and dense gas reservoir/lower SFRs compared to the other simulations; m12w (and to a less dramatic extent m12c, though with the same result) exhibits a dramatic lack of gas in its center (within 1 kpc) due to a massive starburst occurring just before the beginning of our analysis, and only near the end of the $\sim$22 Myr period does the central gas reservoir begin to recover (as a result it does not appear on Figure 3, since it does not simultaneously have SFR and gas tracers within 145 pc). This case is very similar to the gas compaction and inside-out quenching episodes seen in simulations of blue nuggets (that become red nuggets) at higher redshift (Tacchella et al. 2016a, 2016b). These episodes, however, need not be restricted to high-redshift, as observations with ALMA and in the MaNGA Survey (Brownson et al. 2020; Lin et al. 2020) have shown similar variations in central star formation efficiency sans mergers in green valley galaxies in the local universe.

Several of the galaxies match the CMZ observations simultaneously in $\Sigma_{\rm C\&D}$ and $\Sigma_{\rm SFR}$ at some point in this time period, with the galaxies generally exhibiting depletion times on the shorter end of CMZ estimates. Figure 3 demonstrates this, placing the five galaxies that simultaneously have tracers of star formation and cold and dense gas in their central 145 pc on the KS plane (i.e., all but m12c and m12w), and comparing them with appropriate CMZ observations, and spatially resolved observations of M51 (with 170 pc pixels; Blanc et al. 2009) and the Antennae galaxy nuclei (NGC 4038/9, at $\sim$675 pc; Bemis & Wilson 2019).

Interestingly, both m12f, class (a), and significantly lower-mass m12r, class (b), strongly overlap with the Antennae galaxies KS data, suggesting similarities between merger-induced starbursts and self-driven bursty star formation. Indeed, simulation work modeling the Antennae interaction by Renaud et al. (2019) and of mergers more generally in the FIRE-2 suite by Moreno et al. (2020) have shown the dramatic effects that these events can have on the gas reservoirs in the

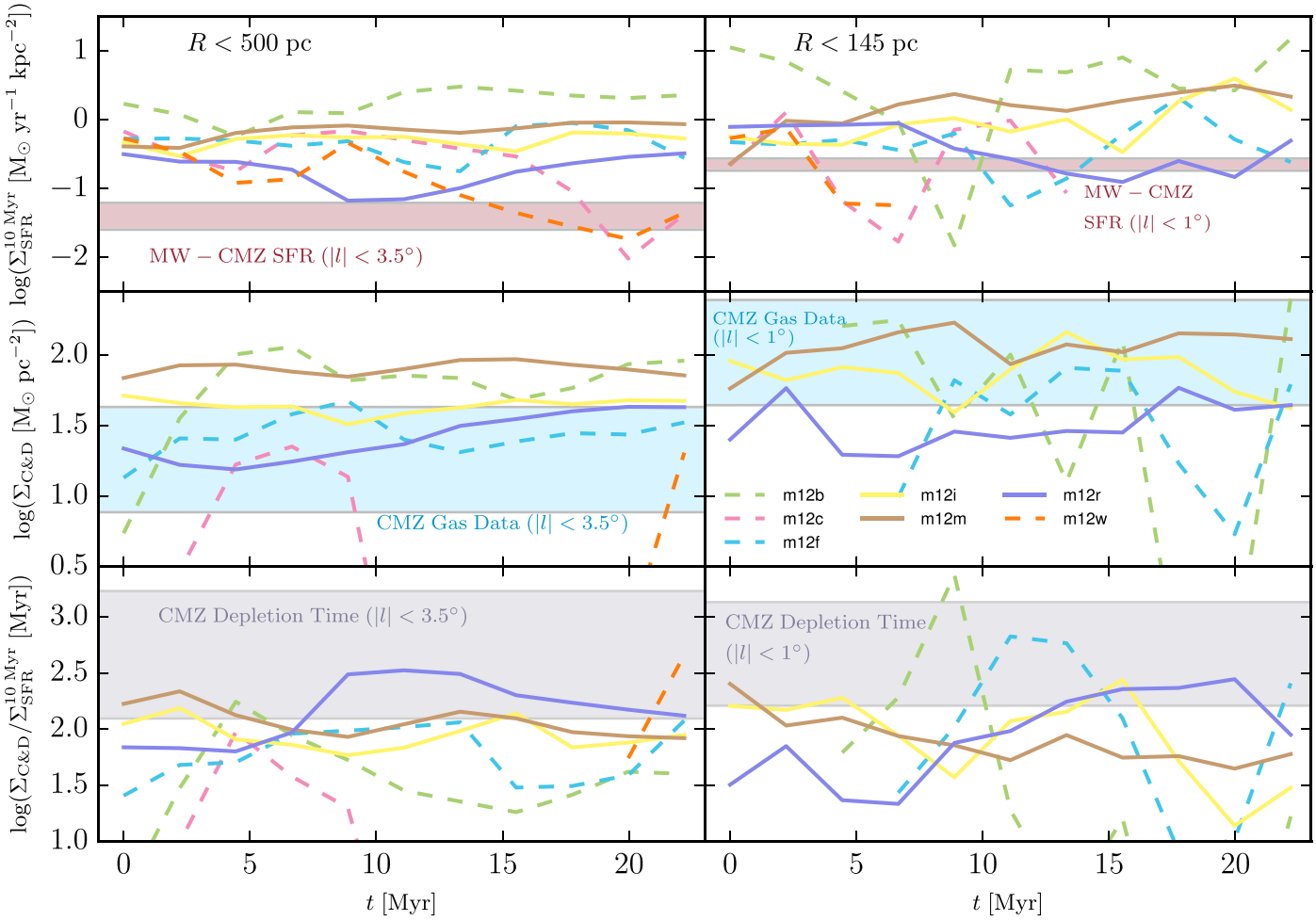

Figure 2. SFRs and cold and dense (C&D) gas surface densities in central regions of seven FIRE-2 spiral galaxies (colored lines; "class (a)/(b)" plotted with dashed/solid lines, respectively), for $R < 500$ (left column) and $R < 145$ pc (right column) apertures, as a function of time near $z \approx 0$ ($\Delta t \approx 2.2$ Myr, rightmost edge being $z = 0$). Shaded bands indicate SFR and gas surface density observations, with uncertainty, of the CMZ from Longmore et al. (2013) and Mills & Battersby (2017), respectively. Depletion times ($\Sigma_{\rm C\&D}/\Sigma_{\rm SFR}^{10\ {\rm Myr}}$) are also presented, in the same style; these CMZ depletion times are produced by combining Longmore et al. (2013) and Mills & Battersby (2017) data. SFRs evolve more smoothly in all galaxies in larger apertures ($R < 500$ pc), and the variance in SFRs or gas surface density increases with smaller apertures. However, in the simulations, two central molecular zone classes appear to exist on $R < 145$ pc scales: galaxies like m12b and m12c with very asymmetric gas distributions and dramatic starbursts on ∼10 Myr timescales, "class (a)"; and galaxies like m12i and m12m typifying smoother (though still with nontrivial fluctuations) SFR and gas distributions in their centers, "class (b)" (see, m12b and m12m in Figure 1 as examples of classes (a) and (b), respectively). Despite temporal and spatial variance, many of the FIRE galaxies are consistent with MW CMZ observations at some point in this time window.

central kiloparsec, and subsequent (∼10 Myr later) central SFRs.

Viewed on the KS relation, the simulations exhibit significantly different tracks over 22 Myr, with, e.g., m12m stationary with a nearly constant SFR and cold and dense gas reservoir, and m12b traveling dramatically across the KS-plane (∼2 dex along either axis). Yet, both of these galaxies at some point overlap with observations of the MW CMZ (which itself has been found to lie on the neutral gas–SFR KS relation; Yusef-Zadeh et al. 2009), or parts of the central region of M51. The SFRs in the class (a) galaxies appear to undergo ≈2 starbursts in the 22 Myr window, consistent with feedback/starburst instability timescales discussed in literature (Kruijssen et al. 2014; Benincasa et al. 2016; Orr et al. 2019). None of the galaxies evolve consistently along lines of constant depletion time: all five shown in Figure 3 exhibit scatter in their centers about $\tau_{\rm dep} \approx \Sigma_{\rm C\&D}/\Sigma_{\rm SFR} \sim 100$ Myr. Though these central regions can exhibit significant time-variability in their SFRs over few-Myr periods, commensurate with YSO/Hα timescales like those of the Longmore et al. (2013) observations, in a time-averaged sense (∼10–100 Myr) they are consistent with the observed KS relation on ∼150 pc scales, modulo observational uncertainties (Orr et al. 2018).

4. Summary and Conclusions

In this Letter, we analyzed the central core regions of seven FIRE-2 Milky Way–mass simulated disk galaxies by spatially mapping their SFRs and gas surface densities, and primarily compared them with comparable observations of the Milky Way CMZ. Our main results are as follows:

1. There are two fairly distinct morphological classes of fiery cores in this sample, with some galaxies exhibiting very asymmetric/clumpy central gas and star formation distributions (class (a)) and others with fairly smooth distributions (class (b)). The intense (concentrated) starbursts in the class (a) cores appear to dramatically alter the gas structures in their centers, whereas the smoother feedback from the star formation cirrus of class (b) cores appear not able to do so.

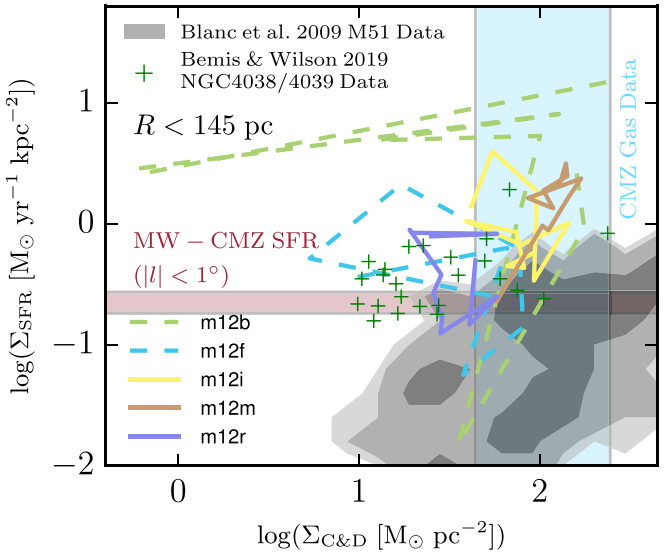

Figure 3. KS relation in central regions of the five FIRE-2 spiral galaxies (colored lines: "asymmetric" centers plotted with dashed lines, "smooth" centers with solid lines) that simultaneously have SFR and dense gas tracers within the $R < 145$ pc aperture, as a function of time near $z \approx 0$ ($\Delta t \approx 2.2$ Myr). CMZ SFR and gas estimates, with uncertainty (Longmore et al. 2013 and Mills & Battersby 2017) plotted as horizontal and vertical shaded bands, respectively, and spatially resolved KS observations (∼170 pc and ∼675, respectively) of M51 (Blanc et al. 2009 their $X_{\rm CO}$ adjusted to be consistent with MW value) and the Antennae Galaxies (NGC 4038/9; Bemis & Wilson 2019) plotted in grayscale contours and with green "+"s, respectively. The central regions of some galaxies remain fairly stable in KS-space over 22 Myr (e.g., m12m), whereas others (e.g., m12b) vary by upwards of a dex in both SFR and $\Sigma_{\rm C\&D}$. Four FIRE galaxies (m12b, m12f, m12m, and m12r) overlap with the CMZ SFR estimate at various times.

2. Even in the absence of tuning the initial properties of any of the simulations, we nonetheless find that four of the galaxies analyzed here (m12b, m12f, m12m, and m12r) are able to match CMZ SFR and gas surface density observations at some point in a 22 Myr period.
3. Intriguingly, of the simulated galaxies that simultaneously match MW CMZ gas and SFR observations, half have asymmetric, time-varying gas and SFR distributions (i.e., are in class (a)), while the other half are fairly smooth class (b) galactic centers. These results demonstrate that a time-varying model can account for the low star formation efficiency (per mass of dense gas) of the CMZ, and that it is not produced solely by some steady-state equilibrium. In fact, the presence of bars and the influence of SMBHs may make class (b) galactic centers untenable in reality.

In all, these simulated galaxies cover a wide range in SFRs and gas surface densities, exhibit marked morphological differences, and some undergo significant changes in the span of only 22 Myr. The simulations lack SMBHs and (strong) bars, and so we cannot comment on the direct role that either of those would play in shaping and/or regulating the core regions of these galaxies. However, this letter highlights (1) the ability of the FIRE-2 zoom-in simulations to reproduce the "large scale" (i.e., 145 pc scale) properties of the CMZ; (2) the marked importance of asymmetric, time-varying (i.e., bursty) star formation and feedback in shaping central galactic regions; (3) that future work with these simulations may help explain how the variety of naturally occurring conditions in central galactic environments arises.

The authors would like to thank Alexander Gurvich, and an anonymous referee, for helpful comments that improved the manuscript. C.B. and H.P.H. gratefully acknowledge support from the National Science Foundation under Award No. 1816715. H.P.H. thanks the LSSTC Data Science Fellowship Program, which is funded by LSSTC, NSF Cybertraining Grant #1829740, the Brinson Foundation, and the Moore Foundation; his participation in the program has benefited this work. The Flatiron Institute is supported by the Simons Foundation. A.W. received support from NASA through ATP grant 80NSSC18K1097 and HST grants GO-14734, AR-15057, AR-15809, and GO-15902 from STScI; the Heising-Simons Foundation; and a Hellman Fellowship. Support for SRL was provided by NASA through Hubble Fellowship grant HST-JF2-51395.001-A awarded by the Space Telescope Science Institute, which is operated by the Association of Universities for Research in Astronomy, Inc., for NASA, under contract NAS5-26555. R.S.K. acknowledges financial support from the German Research Foundation (DFG) via the Collaborative Research Center (SFB 881, Project-ID 138713538) "The Milky Way System" (subprojects A1, B1, B2, and B8). He is also thankful for funding from the Heidelberg Cluster of Excellence STRUCTURES in the framework of Germany's Excellence Strategy (grant EXC-2181/1-390900948) and for funding from the European Research Council via the ERC Synergy Grant ECOGAL (grant 855130).

ORCID iDs

Matthew E. Orr https://orcid.org/0000-0003-1053-3081
H Perry Hatchfield https://orcid.org/0000-0003-0946-4365
Cara Battersby https://orcid.org/0000-0002-6073-9320
Christopher C. Hayward https://orcid.org/0000-0003-4073-3236
Philip F. Hopkins https://orcid.org/0000-0003-3729-1684
Andrew Wetzel https://orcid.org/0000-0003-0603-8942
Samantha M. Benincasa https://orcid.org/0000-0003-4826-9079
Sarah R. Loebman https://orcid.org/0000-0003-3217-5967
Mattia C. Sormani https://orcid.org/0000-0001-6113-6241
Ralf S. Klessen https://orcid.org/0000-0002-0560-3172

References

Anglés-Alcázar, D., Faucher-Giguère, C.-A., Quataert, E., et al. 2017, MNRAS Lett, 472, L109
Armillotta, L., Krumholz, M. R., Di Teodoro, E. M., & McClure-Griffiths, N. M. 2019, MNRAS, 490, 4401
Barnes, A. T., Longmore, S. N., Avison, A., et al. 2019, MNRAS, 486, 283
Barnes, A. T., Longmore, S. N., Battersby, C., et al. 2017, MNRAS, 469, 2263
Bemis, A., & Wilson, C. 2019, AJ, 157, 131
Benincasa, S. M., Loebman, S. R., Wetzel, A., et al. 2020, MNRAS, 497, 3993
Benincasa, S. M., Wadsley, J., Couchman, H. M. P., & Keller, B. W. 2016, MNRAS, 462, 3053
Blanc, G. A., Heiderman, A., Gebhardt, K., Evans, N. J., & Adams, J. 2009, ApJ, 704, 842
Brownson, S., Belfiore, F., Maiolino, R., Lin, L., & Carniani, S. 2020, MNRAS Lett., 498, L66
Casasola, V., Hunt, L., Combes, F., & García-Burillo, S. 2015, A&A, 577, A135
Clark, P. C., Glover, S. C. O., Ragan, S. E., & Duarte-Cabral, A. 2019, MNRAS, 486, 4622
Debattista, V. P., Gonzalez, O. A., Sanderson, R. E., et al. 2019, MNRAS, 485, 5073
Gallagher, M. J., Leroy, A. K., Bigiel, F., et al. 2018, ApJ, 858, 90
Garrison-Kimmel, S., Hopkins, P. F., Wetzel, A., et al. 2018, MNRAS, 481, 4133

Ginsburg, A., Bally, J., Barnes, A., et al. 2018, ApJ, 853, 171
Gurvich, A. B., Faucher-Giguère, C.-A., Richings, A. J., et al. 2020, MNRAS, 498, 3664
Henshaw, J. D., Ginsburg, A., Haworth, T. J., et al. 2019, MNRAS, 485, 2457
Hopkins, P. F., Kereš, D., Onorbe, J., et al. 2014, MNRAS, 445, 581
Hopkins, P. F., Wetzel, A., Kereš, D., et al. 2018, MNRAS, 480, 800
Immer, K., Schuller, F., Omont, A., & Menten, K. M. 2012, A&A, 537, A121
Kennicutt, R. C., & Evans, N. J. 2012, ARA&A, 50, 531
Kennicutt, R. C., Jr 1998, ApJ, 498, 541
Kormendy, J., & Kennicutt, R. C. 2004, ARA&A, 42, 603
Kruijssen, J. M. D., Dale, J. E., & Longmore, S. N. 2015, MNRAS, 447, 1059
Kruijssen, J. M. D., Longmore, S. N., Elmegreen, B. G., et al. 2014, MNRAS, 440, 3370
Krumholz, M. R., & Gnedin, N. Y. 2011, ApJ, 729, 36
Krumholz, M. R., Kruijssen, J. M. D., & Crocker, R. M. 2017, MNRAS, 466, 1213
Lada, C. J., Forbrich, J., Lombardi, M., & Alves, J. F. 2012, ApJ, 745, 190
Lada, C. J., Lombardi, M., & Alves, J. F. 2010, ApJ, 724, 687
Leitherer, C., Schaerer, D., Goldader, J. D., et al. 1999, ApJS, 123, 3
Leroy, A. K., Bolatto, A. D., Ostriker, E. C., et al. 2018, ApJ, 869, 126
Leroy, A. K., Walter, F., Sandstrom, K., et al. 2013, AJ, 146, 19
Liermann, A., Hamann, W.-R., & Oskinova, L. M. 2012, A&A, 540, A14
Lin, L., Ellison, S. L., Pan, H.-A., et al. 2020, ApJ, 903, 145
Longmore, S. N., Bally, J., Testi, L., et al. 2013, MNRAS, 429, 987
Lu, J. R., Do, T., Ghez, A. M., et al. 2013, ApJ, 764, 155
Mills, E. A. C., & Battersby, C. 2017, ApJ, 835, 76
Molinari, S., Bally, J., Noriega-Crespo, A., et al. 2011, ApJ, 735, L33
Moreno, J., Torrey, P., Ellison, S. L., et al. 2020, MNRAS, in press (doi:10.1093/mnras/staa2952)
Orr, M. E., Hayward, C. C., Hopkins, P. F., et al. 2018, MNRAS, 478, 3653
Orr, M. E., Hayward, C. C., & Hopkins, P. F. 2019, MNRAS, 486, 4724
Orr, M. E., Hayward, C. C., Medling, A. M., et al. 2020, MNRAS, 496, 1620
Rathborne, J. M., Longmore, S. N., Jackson, J. M., et al. 2014, ApJ, 786, 140
Renaud, F., Bournaud, F., Agertz, O., et al. 2019, A&A, 625, A65
Sanderson, R. E., Wetzel, A., Loebman, S., et al. 2020, ApJS, 246, 6
Schmidt, M. 1959, ApJ, 129, 243
Sormani, M. C., Binney, J., & Magorrian, J. 2015, MNRAS, 449, 2421
Sormani, M. C., & Li, Z. 2020, MNRAS, 494, 6030
Sormani, M. C., Tress, R. G., Glover, S. C. O., et al. 2020, MNRAS, 497, 5024
Sormani, M. C., Treß, R. G., Ridley, M., et al. 2018, MNRAS, 475, 2383
Tacchella, S., Dekel, A., Carollo, C. M., et al. 2016a, MNRAS, 457, 2790
Tacchella, S., Dekel, A., Marcella Carollo, C., et al. 2016b, MNRAS, 458, 242
Torrey, P., Hopkins, P. F., Faucher-Giguère, C. A., et al. 2017, MNRAS, 467, 2301
Tress, R. G., Sormani, M. C., Glover, S. C. O., et al. 2020, MNRAS, 499, 4455
Velázquez, J. A. F., Gurvich, A. B., Faucher-Giguére, C.-A., et al. 2021, MNRAS, 501, 4812
Walker, D. L., Longmore, S. N., Zhang, Q., et al. 2018, MNRAS, 474, 2373
Wetzel, A. R., Hopkins, P. F., Kim, J.-h., et al. 2016, ApJL, 827, L23
Yusef-Zadeh, F., Hewitt, J. W., Arendt, R. G., et al. 2009, ApJ, 702, 178